Groundwater for Sustainable Development 16 (2022) 100699

Contents lists available at ScienceDirect

Groundwater for Sustainable Development

journal homepage: www.elsevier.com/locate/gsd

Research paper

Adsorptive removal of fluoride from water by chemically modified coal fly ash: Synthesis, characterization, kinetics, and mechanisms

R.A.J.C. Ranasinghe [a], M.A.C.K. Hansima [b], K.G.N. Nanayakkara [a,*]

[a] Department of Civil Engineering, Faculty of Engineering, University of Peradeniya, Kandy, 20400, Sri Lanka
[b] Postgraduate Institute of Science, University of Peradeniya, Kandy, 20400, Sri Lanka

HIGHLIGHTS

- A highly efficient, novel sorbent is synthesized using fly ash for fluoride removal.
- Specific surface area of the sorbent is over 205 m^2g^{-1}.
- Maximum adsorption capacity of 19.8 mg g^{-1} is achieved.
- Based on characterization, mechanisms of sorption process is proposed.

GRAPHICAL ABSTRACT

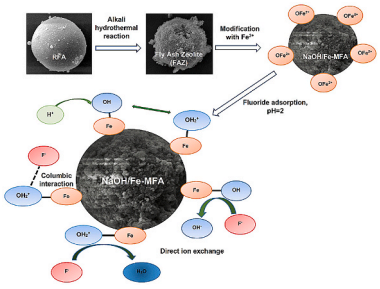

ARTICLE INFO

Keywords:
Adsorption
Fluoride
Chemically modified fly ash
Contaminated water

ABSTRACT

Raw fly ash (RFA) was modified using NaOH and $FeCl_3$ (NaOH/Fe-MFA) to enhance the adsorptive properties for removal of fluoride from water. SEM-EDX, XRD and FTIR, point for zero charge (PZC), specific surface area, and particle size were considered to contrast adsorbent properties of RFA and NaOH/Fe-MFA. The impact of operating variables such that initial solution pH, contact time, adsorbent dosage over fluoride adsorption were evaluated using synthetic water samples. Isotherm and kinetics studies were performed for NaOH/Fe-MFA. Adsorption experiments showed a higher adsorption capacity for NaOH/Fe-MFA over RFA. After 2 h reaction, maximum fluoride removal of 92% was observed with 2 g L^{-1} of NaOH/Fe-MFA at pH 2. At pH 7, under similar conditions, 34% of removal was observed. Fluoride adsorption from NaOH/Fe-MFA was followed Langmuir isotherm, and monolayer fluoride adsorption on homogeneous NaOH/Fe-MFA was confirmed with a considerably high capacity of 18.6 mg g^{-1}. Chemisorption adsorption was revealed from well-fitted kinetics data with pseudo-second-order model. Dominant mechanism for fluoride adsorption from NaOH/Fe-MFA was identified as iron exchange with surface OH^-, which bonds to Fe^{3+} ions.

1. Introduction

Fluoride has both beneficial and adverse impacts on people, and the optimal levels for potable water fluctuate between 0.5 and 1.0 mg L^{-1}, depending mostly on climatic circumstances (WHO, 2004; Kimambo et al., 2019). Low fluoride concentrations in drinking water (<0.5 mg

* Corresponding author.
E-mail addresses: jayani.we18@eng.pdn.ac.lk (R.A.J.C. Ranasinghe), 127charithahansima@gmail.com (M.A.C.K. Hansima), nadeen@eng.pdn.ac.lk, kgnn@pdn.ac.lk (K.G.N. Nanayakkara).

https://doi.org/10.1016/j.gsd.2021.100699
Received 11 August 2020; Received in revised form 25 October 2021; Accepted 28 October 2021
Available online 5 November 2021

L^{-1}) cause male and female fertility issues, dental caries, and human physical growth issues (Kimambo et al., 2019), and high range of fluoride concentrations (>1.5 mg L^{-1}) are the reasons for fluorosis in teeth. If it varies between 3.0 and 6.0 mg L^{-1}, it will result in serious bones disorders (Chandrajith et al., 2012; Ali et al., 2018). Also, high fluoride concentration in irrigation water may cause food crops with high fluoride content (Kut et al., 2016).

Weathering and dissolving of fluoride-containing minerals and fluoride-containing industrial effluents are the main fluoride contamination sources (Jacks et al., 2005; Ali et al., 2019). Over 200 million people over the globe depend on high levels of fluoride-containing water (>1.5 mg L^{-1}) which exceed the present WHO guideline (Vithanage and Bhattacharya, 2015 a). Over 25 countries around the globe have water sources with higher levels of fluoride including Bangladesh, India, Pakistan, Sri Lanka, China, Argentina, Mexico, Finland (Kumar et al., 2016), African countries such as Kenya, Ivory Coast, Ghana and Ethiopia (Kut et al., 2016). Higher fluoride concentrations (>1.0 mg L^{-1}) in drinking water wells have been mainly identified in the northern and southern part of Sri Lanka where more than 8 million people are being suffered due to issues related to fluoride (Chandrajith et al., 2012). According to Dissanayake (2005), in some areas concentrations are high as 10 mg L^{-1} (Dissanayake, 2005).

Among available technologies chemical precipitation/coagulation, membrane filtration, and adsorption are the commonly used treatment techniques to remove high concentrations of fluoride (Vithanage and Bhattacharya, 2015 b; Kut et al., 2016). Among them, adsorption holds an important place in fluoride removal as it is a simple, efficient, economical, and fast treatment technique. Activated carbon (Fito et al., 2019), activated alumina (Vithanage and Bhattacharya, 2015 a), activated fly ash (Geethamani et al., 2014), zeolite (Waghmare et al., 2015) and related ion exchangers (Sun et al., 2011) are the most widely used adsorbents to treat water with higher fluoride concentrations.

Fly ash (FA) is abundant industrial waste material and over 750 million tons of FA has been generated per annum during coal combustion (Noor-ul-Amin, 2014). China (50.8%), the USA (15.2%), India (13.5%), Europe (6.8%), Africa, and the Middle East (4.1%) are the regions where major production of fly ash is taken place (Ahmed et al., 2016). In Sri Lanka, 165 tons of FA is generated per annum in the Norochcholai coal-fired power plant while a small portion, about 20%, is utilized for cement production (Venuja et al., 2017). FA can be identified as a low-cost material with good adsorption properties (Visa et al., 2012). Adsorption properties of FA can be improved by chemical modifications. Studies show that alkali modified FA has good adsorptive properties for removing contaminants including fluoride (Geethamani et al., 2014), dyes (Sahoo et al., 2013), ammonium (Makgabutlane et al., 2020), and heavy metals (Visa et al., 2012) from aqueous solutions. FA converts into zeolites minerals after chemical modification using alkalis, such as NaOH (Koshy and Singh, 2016). Chemical constitution of FA, alkaline aqueous solution concentration, FA to liquid ratio, temperature, pressure, and reaction time were identified as the main concerns on the mineralogy of the alkali modified FA (Prasad et al., 2011). Zeolite skeletal structure is made of alumina and silica tetrahedra and thus high levels of negative charge can be identified on the surface of the zeolite structure which is generated from oxygen atoms of alumina and silica tetrahedra. Since the affinity towards anion is very less due to the negatively charged surface of zeolite, transition metal cations can be used to improve the zeolite surface for anion removal (Sun et al., 2011).

This investigation was implemented to synthesize a low-cost novel adsorbent to adsorb fluoride from water by chemical modification of raw fly ash (RFA) using NaOH followed by Fe^{3+} ions (NaOH/Fe-MFA). Further, properties of RFA and NaOH/Fe-MFA were compared using SEM-EDX, XRD, FTIR analysis, point for zero charge (PZC), specific surface area, and other related characteristics. The impacts of operating parameters (pH, time, adsorbent dosage) were investigated. Maximum adsorption capacity, rate, and order of the adsorption reactions were examined by using adsorption isotherm and kinetics. Further, possible mechanisms for fluoride adsorption by NaOH/Fe-MFA have been explored.

2. Materials and methodologies

2.1. Materials

Norochcholei coal power plant (Sri Lanka) is generating a considerable amount of FA and those were considered as the raw material. Analytical grade sodium hydroxide (NaOH), anhydrous ferric chloride ($FeCl_3$), anhydrous sodium fluoride (NaF), and hydrochloric acid (HCl) was used. HACH fluoride SPADNS reagent was used to measure fluoride concentrations. Whatman normal filter papers were used to filter water samples after adsorption experiments.

2.2. Preparation of adsorbents

2.2.1. Raw fly ash (RFA)

FA was washed thoroughly using distilled water (3 times). Then it was mixed with water for 30 min using a magnetic stirrer and it was precipitated. The supernatant was removed, and the precipitate was dried in an oven at 100 ± 5 °C. Then it was cooled to ambient temperature and categorized using a 75-μm mesh.

2.2.2. Chemically modified fly ash (NaOH/Fe-MFA)

The modification was done in two steps.

Step 1 –Fly Ash Zeolite (FAZ).

Alkali modification of RFA was performed similarly to a method reported in the literature (Prasad et al., 2011) to prepare FAZ as the intermediate material. Prepared RFA was mixed with 2 mol L^{-1} NaOH solution while maintaining RFA sample to solution ratio as 1:5. The open reflux method was used at 95 °C for 24 h to proceed with the conversion reaction. Then the sample was washed and filtered repeatedly, and simultaneously electrical conductivity (EC) and pH of wash water were measured until it reaches a constant value. After washing, the sample was oven-dried at 45–50 °C until it reached a constant weight. Finally, it was crushed using a ceramic mortar.

Step 2 - Chemically modified fly ash (NaOH/Fe-MFA).

FAZ was further modified with Fe^{3+} as the method proposed by Abaei et al. (2017) with some slight modifications (Abaei et al., 2017) to reduce the negative charge on FAZ surface. By using the open reflux method 0.3 mol L^{-1} $FeCl_3$ sample and prepared FAZ was reacted for 48 h at 45 °C while maintaining sample to solution ratio 1:10. Then, by using distilled water the sample was washed and filtered repeatedly until pH and EC of wash water reach a constant value. The washed sample was dried at 100 ± 5 °C and monitored till the sample weight become constant. Subsequently, it was cooled to room temperature and crushed using a ceramic mortar.

2.3. Characterization of adsorbents

SEM-EDX analysis with the use of a Scanning Electron microscope (EVO LS 15) was used to characterize changes in surface morphology and chemical composition. Changes in crystalline structures were analyzed using Bruker D8 Focus X-Ray Diffractometer. Surface chemical bonds and functional groups present in adsorbents before and after adsorption experiments were determined using Bruker Vertex 80 FTIR Spectrometer. Particle size distribution was measured using FRITSCH Analysette 22 MicroTec plus particle size analyzer (range: 0.08 μm–2000 μm). Micrometrics TriStar II Surface Area and Porosity analyzer with N_2 adsorption at low operating temperature (−195.8 °C) was used to determine Brunauer, Emmet, and Teller (BET) specific surface area (SS_{BET}). Conversion gas volume model was used to determine pore distribution. Point for zero charge (PZC) was determined using the batch equilibrium approach (Pathiraja et al., 2015).

2.4. Batch experiments

Fluoride adsorption onto RFA and NaOH/Fe-MFA were investigated as batch experiments using synthetic water samples. Impacts of initial solution pH, contact time, adsorbent dosage on fluoride adsorption were evaluated with 10 mg L^{-1} stock solution. Isotherm and kinetics were studied for NaOH/Fe-MFA. The required pH adjustments for the batch experiments were performed by using HCl and NaOH solutions. Adsorption reactions were performed with known quantities of adsorbents and 25 ml working volume of fluoride solutions using a lab shaker with a speed of 200 rpm. At the end of the reaction, to measure the residual concentration HACH DR 900 multi-parameter portable colorimeter was used. All aforesaid experiments were performed thrice at room temperature. Standard deviations were used to measure the standard errors. In all graphs, standard error bars were incorporated. Fluoride removal was calculated using Equation (1) and Equation (2):

$$q_e = \frac{(C_0 - C_{eq})V}{W} \quad (1)$$

$$E(\%) = \frac{(C_0 - C_{eq}) * 100}{C_0} \quad (2)$$

where V, W, C_0, C_{eq}, q_e, E(%) represent solution volume (mL), weight of adsorbent added (g), initial fluoride concentration (mg L^{-1}), equilibrium concentration (mg L^{-1}), adsorption capacity at equilibrium (mg g^{-1}) and fluoride removal efficiency (%) respectively.

3. Results and discussion

Results of material characterization and batch experiments and possible mechanisms for fluoride adsorption by NaOH/Fe-MFA were discussed below.

3.1. Characterization

3.1.1. Scanning Electron microscopy – electron dispersive X-ray (SEM-EDX)

Fig. 1 depicts SEM photographs of RFA and NaOH/Fe-MFA. Fig. 1(a) & (b) indicate RFA particles are spherical and have a smooth surface. As Fig. 1(c) & (d) depict NaOH/Fe-MFA particles are highly irregular in shape and have more voids and holes on the surface which increases the available surface for adsorption.

Base on the obtained results from EDX analysis (Table 1) major components of RFA are oxides of Si, Al, Ca, Ti and Fe. Silicon dioxide (SiO_2) and aluminium oxide (Al_2O_3) composition of RFA is about 92% of the total mass (SiO_2+Al_2O_3 = 92.45%) and the total percentage of other oxides are less than 10%. The smooth surface of RFA is a result of this alumina-silicate glass phase (Makgabutlane et al., 2020). Major components of NaOH/Fe-MFA are oxides of Si, Al, Ca, Fe and Mg. NaOH/Fe-MFA has a higher percentage of FeO, a lesser percentage of Al_2O_3, SiO_2 and CaO compared to RFA. The higher percentage of FeO is due to the surface bonding of Fe^{3+} through chemical modification. The lesser percentage of Al_2O_3 and SiO_2 is due to the dissolution of aluminosilicate during alkali modification (alkaline hydrothermal reaction) (Panda et al., 2018).

3.1.2. X-ray diffraction (XRD) analysis

Base on the XRD analysis (Fig. 2) of RFA, FAZ, and NaOH/Fe-MFA, through a comparative study, the phase changes of adsorbents after each modification can be observed. The existence of a Na–P1 zeolitic phase in FAZ was determined based on the most intense d-spacing (d = 7.16, 5.05, 4.46, and 3.18 Å) which confirms the formation of zeolite

Table 1
Change in surface chemical compositions of adsorbents from EDX analysis.

Properties (wt %)	Al_2O_3	SiO_2	CaO	TiO_2	FeO	MgO
RFA	41.11	51.34	5.24	1.16	1.15	–
NaOH/Fe-MFA	28.78	35.91	0.23	–	32.08	0.54

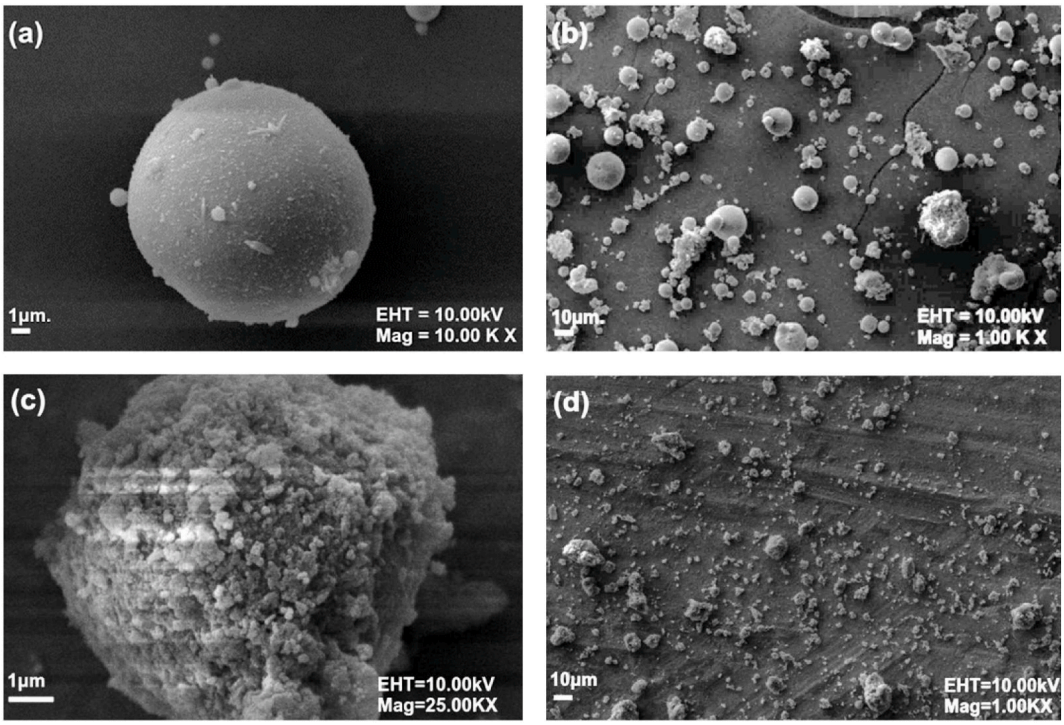

Fig. 1. SEM photographs of (a) & (b) RFA (c) & (d) NaOH/Fe-MFA.

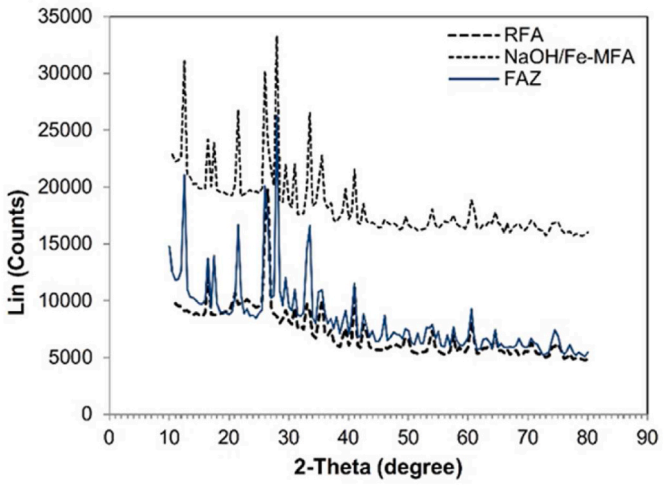

Fig. 2. XRD spectrums of RFA, FAZ and NaOH/Fe-MFA.

through the NaOH modification (Treacy and Higgins, 2001).

The diffraction peak position of NaOH/Fe-MFA is basically same as FAZ, indicating that no crystalline transformation occurred during $FeCl_3$ modification. This confirmed the reaction between $FeCl_3$ and FAZ does not change the original structure of FAZ. However, EDX analysis indicated a higher percentage of FeO on the NaOH/Fe-MFA surface. Thus, the deposited iron oxide can be identified as amorphous, since the XRD pattern of NaOH/Fe-MFA did not show any additional crystalline phases for iron oxides.

3.1.3. Fourier transform infrared spectroscopy (FTIR)

FTIR spectra of RFA and NaOH/Fe-MFA are shown in Fig. 3. Four Major peaks can be identified at 1488, 1067, 877, 737, and 621 cm^{-1} for RFA. The existence of C–O stretching for carbonate which confirms the presence of calcite is indicated by peaks at 877 and 1488 cm^{-1} (Coates, 2000). The existence of Si–O–Si functional groups which confirm the presence of quartz is indicated by the spike at 1067 cm^{-1} (Clara & Kumar, 2016). Existence of Si–O–Al bridges confirms the presence of mullite and it is indicated by the peak at 737 cm^{-1} (Mozgawa et al., 2014). It is identified that spike at 621 cm^{-1} is affected by the contribution of quartz (SiO_2) and mullite ($Al_{5\cdot65}Si_{0\cdot35}O_{9.175}$) due to O–Si–O and O–Al–O bending vibrations (Apua and Simatea, 2018). According to the above analysis, the major components of RFA are calcite, quartz, and mullite.

As per Fig. 3, six major peaks can be identified at 3361, 1637, 1037, 903, 737, and 621 cm^{-1} for NaOH/Fe-MFA. The existence of a higher percentage of O–H stretch (Si–OH, Si–OH–Al, and –OH groups) is indicated by strong and board new peak at 3361 cm^{-1} (Rondón et al., 2013). The existence of Si–O bond is indicated by spike at 1637 cm^{-1}. Then the existence of O–Si–O asymmetric stretching is identified by peak at 1037 cm^{-1} (Prasetyo and Soegijono, 2018). The spike at 903 cm^{-1} is linked to vibrations of Al–O or Al–OH groups (Mozgawa et al., 2014). The external Si–O/Al–O (Fe–O) bends, which indicate surface bonding of Fe^{3+} ions, are responsible for the spike at 737 cm^{-1}. (Suhartana et al., 2018). Bending vibrations of O–Si–O is responsible for spike at 621 cm^{-1} (Byrappa & Kumar, 2007).

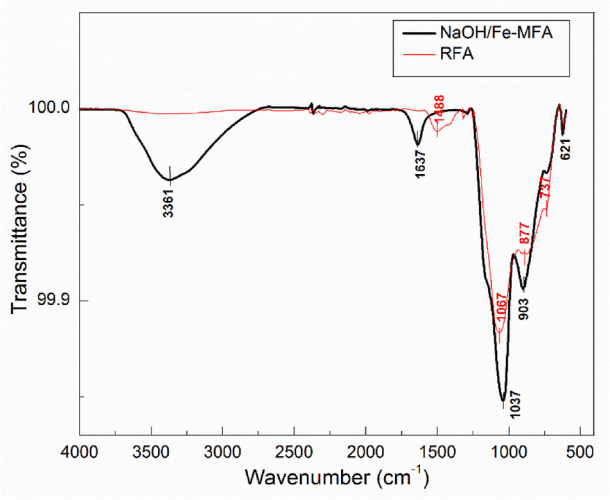

Fig. 3. FTIR spectrums of RFA and NaOH/Fe-MFA.

3.1.4. Physical characterization

Mean particle diameter, SS_{BET}, pore structure, and PZC of adsorbents appear in Table 2. Accordingly, RFA particles are smaller in size compared to NaOH/Fe-MFA. Low SS_{BET} of RFA reveals the requirement of surface modification since adsorption is a surface phenomenon. A significant increase in SS_{BET} can be observed in NaOH/Fe-MFA which indicates the positive impact of chemical modification. This is due to the increased in pore volume and change in mineral composition after chemical modification (Sahoo et al., 2013). NaOH/Fe-MFA has a higher SS_{BET} compared to other chemically modified fly ash adsorbents reported in the literature such as sulfuric acid-modified fly ash (13.4821 m^2g^1) (Qiu et al., 2016), coal fly ash/$CoFe_2O_4$ magnetic composite (58.16 m^2g^{-1}) (Zhang et al., 2016), and HCl-treated fly ash (61.84 m^2g^{-1}) (Pengthamkeerati et al., 2008). Pore volume has increased from 6.091 $\times$ 10^{-4} cm^3g^{-1} (RFA) to 0.0894 cm^3g^{-1} (NaOH/Fe-MFA). Since, Si and Al composition of materials are inversely related to the pore volume (Sahoo et al., 2013), the increased in pore volume of NaOH/Fe-MFA is due to the reduction in Si and Al composition as indicated by EDX analysis (Table 1). There is no considerable change in the pore radius. After modification PZC has changed from 10.45 for RFA to 6.69 for NaOH/Fe-MFA. This reduction is mainly due to the surface bonding of Fe^{3+} which increases the positively charged surface functional groups. Surface of a particle is charged negatively when pH > PZC and charged positively when pH < PZC. The strength of the surface charge increases with the increase of pH difference between solution pH and PZC. Thus lower PZC of NaOH/Fe-MFA indicates that it would be a better adsorbent for fluoride removal compared to RFA.

3.1.5. Chemical reactions during modification

The existence of a Na–P1 zeolitic phase in FAZ confirms the formation of zeolite through the NaOH modification (Equation (3)).

$$Fly\ ash + 2\ mol\ L^{-1}\ NaOH \xrightarrow{95\ ^0C/\ 24\ hrs} Fly\ ash\ zeolite + residuum \quad (3)$$

The changed in PZC confirmed the increase in positive charge of the NaOH/Fe-MFA surface. Further, EDX analysis indicated a higher percentage of FeO on the NaOH/Fe-MFA surface. XRD analysis confirmed, the reaction of $FeCl_3$ with FAZ did not change the original structure of FAZ. Thus, only surface modification has occurred during the modification process.

On the FAZ surface, functional groups like $\equiv ZOH_2^+$, $\equiv ZOH$, and $\equiv ZO^-$ exist. During the $FeCl_3$ modification, the reaction medium was

Table 2
Physical characterization of RFA and NaOH/Fe-MFA.

Sample	Mean particle diameter (μm)	BET Specific surface area (SS_{BET}) ($m^2\ g^{-1}$)	Pore volume ($cm^3\ g^{-1}$)	Pore radius (nm)	Point for zero charge (PZC)
RFA	21.8	1.37	6.091 × 10^{-4}	0.8878	10.45
NaOH/Fe-MFA	30.2	205.68	0.0894	0.8693	6.69

acidic and Fe^{3+} ions are dominant in the medium. Electrostatic attraction forces between negative $\equiv ZO^-$ surface sites and positive Fe^{3+} ions form $\equiv$Z-OFe^{2+} sites to increase the positive charge of zeolite surface by overriding electrostatic repulsion by positive $\equiv ZOH^{2+}$ sites to Fe^{3+} ions.

$$\equiv Z - O^- + Fe^{3+} \rightarrow \equiv Z - OFe^{2+} \quad (4)$$

3.2. Batch experiments

Results of lab experiments for fluoride adsorption onto RFA and NaOH/Fe-MFA were discussed below.

3.2.1. Influence of initial solution pH (pH_i)

Fluoride removals of RFA and NaOH/Fe-MFA against different pH_i values (2–12) with a reaction time of 6 h were illustrated in Fig. 4. Based on the results it is identified that fluoride removal using both adsorbents is highly impacted by pH_i. For both adsorbents, removal efficiencies decrease with the increase of pH_i and maximum removal occurs at pH 2. NaOH/Fe-MFA shows higher removal efficiencies compared to RFA indicating the positive impact of the surface modification. This is mainly due to the increase of SS_{BET}, pore-volume, and surface chemical composition of NaOH/Fe-MFA which provide more active sites for fluoride adsorption. Change in removal efficiencies with pH_i can be explained using PZC as explained in section 3.1.4. When pH_i < PZC, surface of adsorbent particles is charged positively which initiates an attraction force between fluoride ions and adsorbent particles. Higher removal efficiencies at lower pH_i values were due to this reason. When pH_i > PZC, both fluoride ions and adsorbent particles are charged negatively which initiates a repulsive force that result a lower fluoride removal. Another cause for the reduction in removal efficiencies in alkaline pH_i values was the rivalry for adsorption sites between fluoride and OH^- ions, as fluoride ion is identical to OH^- ion in terms of ionic radius and charge. (Xu et al., 2011). Thus, pH 2 was used as the optimum pH_i for both adsorbents.

3.2.2. Influence of contact time (t)

Influence of contact time on fluoride removal at optimum pH_i was investigated from 0 to 150 min and is depicted in Fig. 5. Rapid fluoride adsorption can be seen within the first 5 min. Thereafter, a lower adsorption rate followed by an equilibrium state can be observed. Fluoride adsorption on to outer surface (Geethamani et al., 2014), high solute gradient induced high driving force and availability of abundant active sites (Makgabutlane et al., 2020) were the reasons for the rapid adsorption. The subsequent lower adsorption rate was due to the adsorption that took place inside the pores and the generation of

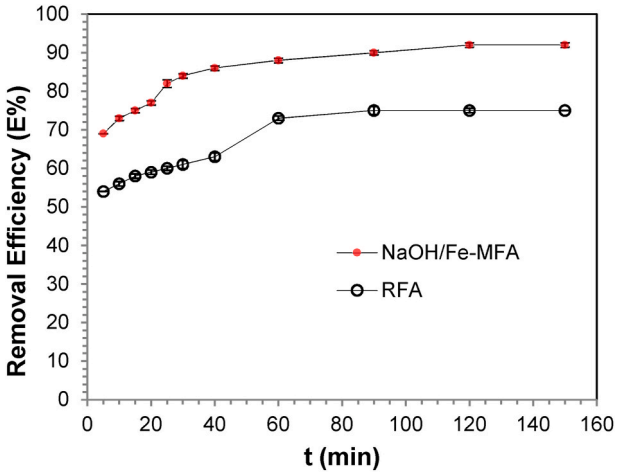

Fig. 5. Influence of contact time on fluoride removal (adsorbent dosage = 2 g L^{-1}; T = 28 °C; pH_i = 2; C_0 = 10 mg L^{-1}).

repulsion between fluoride ions on the adsorbent and in the solution (Geethamani et al., 2014). Time required to reach equilibrium was found as 90 min for RFA and 120 min for NaOH/Fe-MFA. This higher equilibrium time of NaOH/Fe-MFA was due to the larger particle diameter since the equilibrium time of an adsorbent depends on the particle diameter (Worch, 2012).

3.2.3. Influence of adsorbent dosage

Influence of adsorbent dosage on removal efficiencies and adsorption capacities (q_e) is shown in Fig. 6. Equilibrium contact time and optimum pH_i were considered when conducting the experiments. The ability of both adsorbents to absorb fluoride decreases as the adsorbent dosage is increased, which is owing to the existence of more bonding sites for a limited amount of fluoride (Xu et al., 2011). Maximal fluoride removal of RFA was observed as 81% at a dosage of 2.8 g L^{-1} and 92% was observed for NaOH/Fe-MFA at a dosage of 2 g L^{-1}. Thus, optimum adsorbent dosages of RFA and NaOH/Fe-MFA for fluoride removal are 2.8 and 2.0 g L^{-1}. At optimum conditions q_e of RFA and NaOH/Fe-MFA are 3.07 and 4.6 mg g^{-1} which confirms the better applicability of NaOH/Fe-MFA over RFA.

3.2.4. Fourier transform infrared spectroscopy (FTIR)

3.2.4.1. Fluoride adsorbed RFA (F-RFA). FTIR spectra in Fig. 7 (a) reveal the changes in the absorption bands of virgin RFA due to fluoride

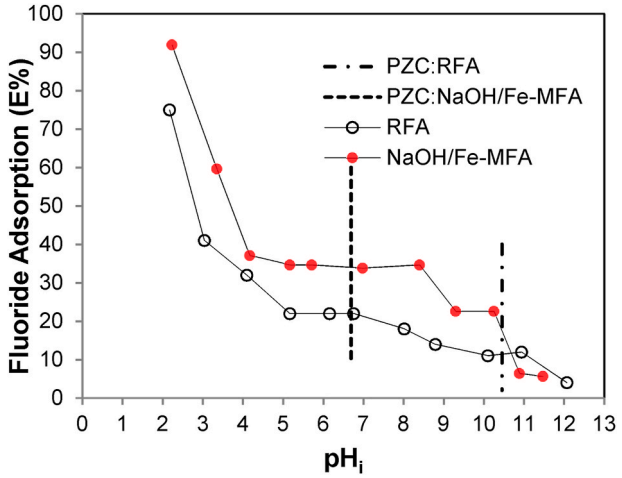

Fig. 4. Influence of pH_i on fluoride removal (C_0 = 10 mg L^{-1}; temperature (T) = 28 °C; contact time (t) = 6 h; adsorbent dosage = 2 g L^{-1}).

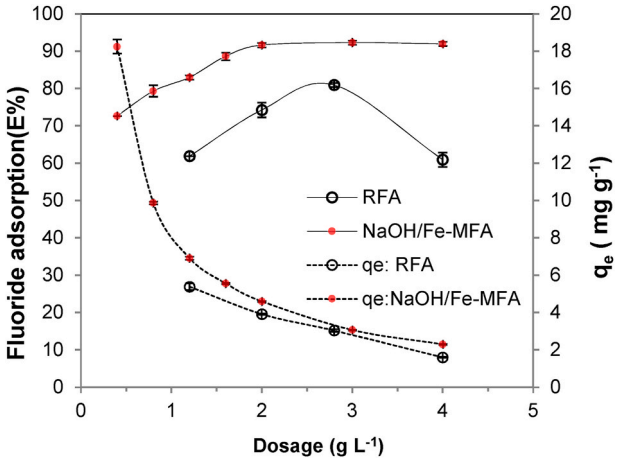

Fig. 6. Influence of adsorbent dosage on fluoride adsorption (T = 28 °C; pH = 2; t = 2 h; C_0 = 10 mg L^{-1}).

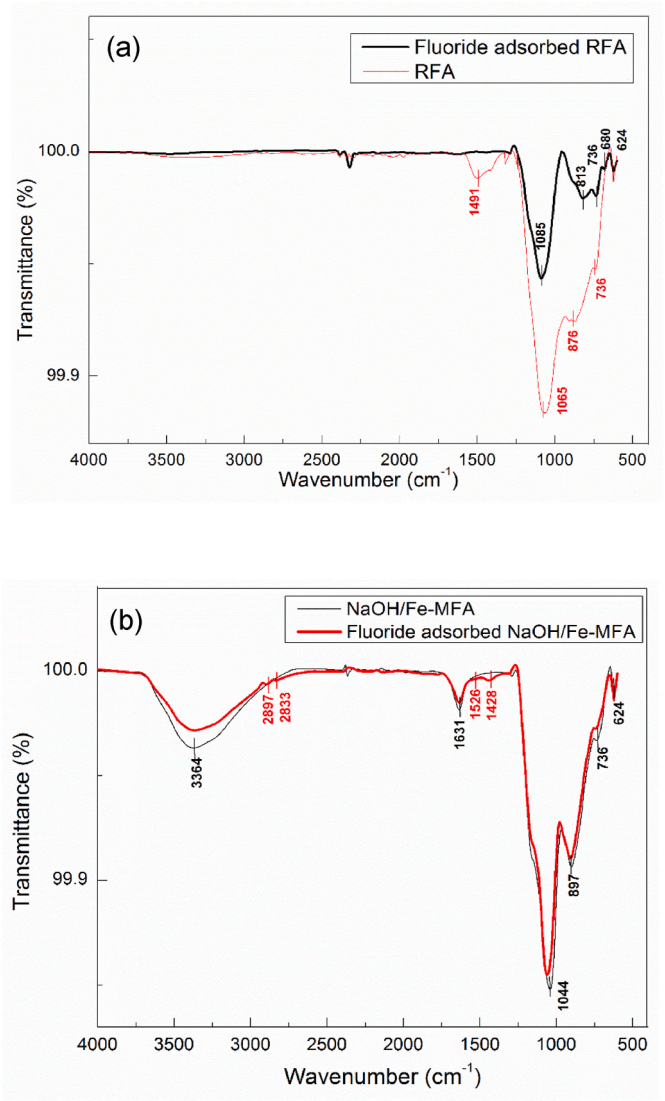

Fig. 7. Pre and post adsorption FTIR spectra of (a) RFA (b) NaOH/Fe-MFA.

adsorption. According to the spectra, calcite exists only in virgin RFA. This was due to the precipitation of fluoride as CaF_2 during adsorption (Nie et al., 2014; Mondal et al., 2016). The intensities (depth of the band) of peaks at 1065, 736, and 624 cm^{-1} have reduced and new peaks have appeared at 813 and 680 cm^{-1} after fluoride adsorption compared to virgin RFA. This data provides evidence of fluoride adsorption.

3.2.4.2. Fluoride adsorbed NaOH/Fe-MFA. FTIR spectra in Fig. 7 (b) reveal the changes in the absorption bands of virgin NaOH/Fe-MFA due to fluoride adsorption. All the absorption peaks of virgin NaOH/Fe-MFA show minor shifts in frequencies after fluoride adsorption. The intensities of peaks can be used to compare the abundance of the functional groups. The intensity of O–H band (depth of the band) has reduced after fluoride adsorption. This was due to fluoride adsorption onto NaOH/Fe-MFA by replacing the OH^- which is similar in size and charge of F^- (Xu et al., 2011) also this replacement makes easier due to the higher affinity of F^- towards Fe (Jayarathna et al., 2015). The spike at 736 cm^{-1} which indicates external Si–O/Al–O (Fe–O) bends has a narrower peak compared to virgin NaOH/Fe-MFA. This may be due to the changes in Si–O/Al–O (Fe–O) bonding by fluoride adsorption. The existence of isolated OH groups after the adsorption can be identified through the appearance of the new weak band around 2897–2833 and 1526-1428 cm^{-1}. This was due to the weakened hydrogen bonding strength causes by the attachment of F^- replacing OH groups bound to Fe (Jayarathna et al., 2015). Above data provide evidence of the fluoride adsorption by NaOH/Fe-MFA.

3.2.5. Adsorption isotherm studies

Maximum adsorption capacities and the interaction of fluoride with adsorbents were studied by using isotherm studies. (Geethamani et al., 2014).

Monolayer adsorption process on a homogeneous surface without lateral interactions between molecules that have been adsorbed is confirmed by Langmuir model. (Maity et al., 2018). The linearized Langmuir equation is shown in Equation (5).

$$\frac{1}{q_e} = \frac{1}{q_m} + \frac{1}{q_m k_a C_e} \tag{5}$$

where q_m, q_e, represent maximum monolayer and equilibrium state adsorption capacities (mg g^{-1}), C_e, k_a represent fluoride concentration at equilibrium (mg L^{-1}) and constant relating to bond formation energy (L mg^{-1}) respectively. The equation of dimensionless separation parameter (R_L) is calculated using Equation (6) (Xu et al., 2011).

$$R_L = \frac{1}{1 + k_a C_0} \tag{6}$$

Multilinear adsorption on a heterogeneous surface is confirmed by Freundlich model (Xu et al., 2011). The linearized Freundlich equation is given in Equation (7).

$$\log q_e = \log k_f + \frac{\log C_e}{n} \tag{7}$$

where k_f, n (heterogeneity factor) represent coefficient relating to adsorption capacity (mg g^{-1}) and intensity respectively (Pathiraja et al., 2015).

Equilibrium studies were conducted for NaOH/Fe-MFA at the optimum conditions by changing initial fluoride concentrations. Adsorption parameters of isotherm models for NaOH/Fe-MFA on fluoride adsorption are represented in Fig. 8 and Table 3. The correlation coefficient (R^2) value for Langmuir model is closer to one when contrasted to Freundlich model. Thus, the experimental data fit Langmuir isotherm well, confirming monolayer fluoride adsorption on a homogenous NaOH/Fe-MFA surface (Aljeboree et al., 2014) with q_m of 18.6 mg g^{-1}. The computed R_L value is 0.237, which lies between 0 and 1, demonstrating a favorable Langmuir adsorption (Xu et al., 2011). Equilibrium adsorption capacities reported in the literature for fluoride removal are compared with the capacity of this study in Table 4. The results demonstrated that NaOH/Fe-MFA is a potential fluoride removal adsorbent.

3.2.6. Kinetics studies

Rate and mechanism of fluoride adsorption were studied using kinetics and linearized pseudo-first-order (PFO) and pseudo-second-order (PSO) reaction models are stated in Equations (8) and (9) (Largittea and Pasquier, 2016).

$$\ln(q_e - q_t) = lnq_e - k_1 t \tag{8}$$

$$\frac{t}{q_t} = \frac{1}{k_2 q_e^2} + \frac{1}{q_e} t \tag{9}$$

where t represents time (min), q_t, q_e represent amount fluoride adsorbed (mg g^{-1}) at time t and equilibrium and k_1, k_2 represent rate constant relevant to PFO adsorption (min^{-1}) and PSO adsorption (g mg^{-1} min^{-1}) respectively.

Equation (10) indicates mathematical expression of Intra Particle diffusion (IPD) model. If the graph of q_t vs. $t^{0.5}$ is linear, it will confirm an IPD process. If it goes through the originator, IPD is the only rate-limiting process. Usually, this plot shows multi-linearity over the

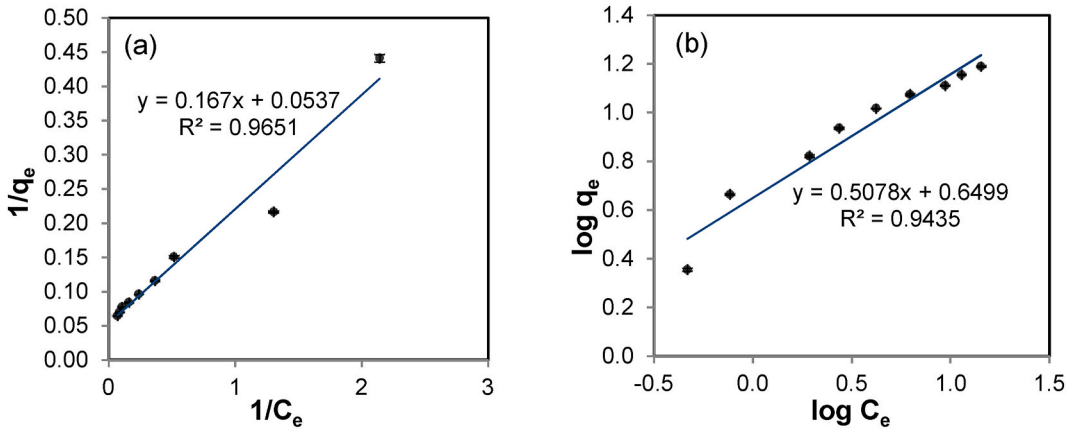

Fig. 8. Plot of isotherms for NaOH/Fe-MFA: (a) Langmuir (b) Freundlich.

Table 3
Isotherm parameters for NaOH/Fe-MFA on fluoride removal.

Isotherm	Langmuir				Freundlich		
Parameter	q_m	k_a	R_L	R^2	k_f	n	R^2
Value	18.6 mg g^{-1}	0.322 L mg^{-1}	0.237	0.97	4.47 mg g^{-1}	1.969	0.94

Table 4
Fluoride removal capabilities of several adsorbents.

Adsorbent	q_m (mg g^{-1})	
Natural stilbite zeolite modified with Fe (III)	2.31	Sun et al. (2011)
Calcium Hydroxide treated fly ash	10.86	Geethamani et al. (2014)
Modified Zeolite	8.03	Waghmare et al. (2015)
Aluminium oxides coated pumic	12.29	Salifu (2017)
Fired Clay Pots	4.16	Kofa et al. (2017)
Bacterial-surfactin mediated novel hydroxyapatite nanoparticle	7.004	Maity et al. (2018)
Catha edulis activated carbon (CAC)	18	Fito et al. (2019)
Fly ash zeolite modified with Fe (III) (NaOH/Fe-MFA)	18.62	This study

entire adsorption period indicating that the process is controlled by various mechanisms (Tan and Hameed, 2017).

$$q_t = k_{id}\sqrt{t} + B \tag{10}$$

where k_{id} and B represent a constant correlated with IPD rate (mg g^{-1} $min^{-0.5}$) and mass transfer across boundary layer (mg g^{-1}) (Elessawy et al., 2020).

Kinetic studies of NaOH/Fe-MFA were conducted at optimum pH_i with the optimum adsorbent dosage using a 10 mg L^{-1} stock solution. Residual fluoride content was determined using the samples taken at appropriate time intervals. Table 5 and Fig. 9 show the analysis of experimental data using linearized PFO and PSO kinetics. Chemisorption adsorption process was revealed from the well-fitted kinetics data with PSO model (Geethamani et al., 2014). Further, the closer value of experimental q_e and theoretical q_e obtained using PSO model confirms the better applicability of PSO model.

Table 5
Kinetic parameters of NaOH/Fe-MFA on fluoride adsorption.

Kinetic model	PFO			PSO		
Parameter	q_e	k_1	R^2	q_e	k_2	R^2
	1.57 mg g^{-1}	0.0346 min^{-1}	0.823	4.69 mg g^{-1}	0.0648 min^{-1}	0.9996

IPD plot is multilinear (three linear segments) over the whole time range (Fig. 10), which indicates the involvement of multiple mechanisms for fluoride adsorption. The outer surface adsorption occurs in the first sharpen zone then IPD begins, and finally the system reaches equilibrium (Geethamani et al., 2014; Tan and Hameed, 2017).

3.2.7. Adsorption mechanisms

The active metal sites (M = Fe^{3+}, Al^{3+}, Mg^{2+}) on the NaOH/Fe-MFA surface convert into oxyhydroxides in aqueous medium. Thus, below reactions can be used to describe the fluoride removal at pH 2 (acidic medium).

$$\equiv Z - MOH + H^+ \leftrightarrow \equiv Z - MOH_2^+ \tag{11}$$

The reactions below show fluoride adsorption by direct ion exchange.

$$\equiv Z - MOH + F^- \leftrightarrow \equiv Z - MF + OH^- \tag{12}$$

$$\equiv Z - MOH_2^+ + F^- \leftrightarrow \equiv Z - MF + H_2O \tag{13}$$

Or they could interact with each other by a non-specific columbic reaction as shown below.

$$\equiv Z - MOH_2^+ + F^- \leftrightarrow \equiv Z - MOH_2^+ \cdots F^- \tag{14}$$

The mechanism of the fluoride adsorption on zeolitic adsorbents has been outlined similarly by Sun et al. (2011) and Tian & Gan. (2019) (Sun et al., 2011; Tian and Gan, 2019). As the radius and ionic charge of F^- and OH^- are similar, this allows the fluoride ions to approach the NaOH/Fe-MFA easily (Xu et al., 2011; Jayarathna et al., 2015).

Equation (15) explains the surface precipitation of fluoride ions as CaF_2, which is possible in alkaline medium (Nie et al., 2014; Mondal et al., 2016). This mechanism is unlikely to occur since EDX results show a minor amount (0.23% by weight) of calcium on NaOH/Fe-MFA surface.

$$\equiv Z - CaCO_3 + 2F^- \rightarrow \equiv Z - CaF_2 + CO_3^{2-} \tag{15}$$

According to the literature sorption within pores is possible only when the pore size of adsorbent is greater than 1.7 times of the adsorbate's second broadest dimension (Peiris et al., 2019). Thus, fluoride adsorption inside the pore is conceivable to occur since pore radius of NaOH/Fe-MFA is more than six times larger compared to the ionic radius of fluoride (1.36 Å) (Yehia and Ezzat, 2009).

Adsorption kinetic studies confirmed that fluoride adsorption by NaOH/Fe-MFA was controlled by chemisorption. Therefore, the direct ion-exchange mechanism explained by equations (12) and (13) can be

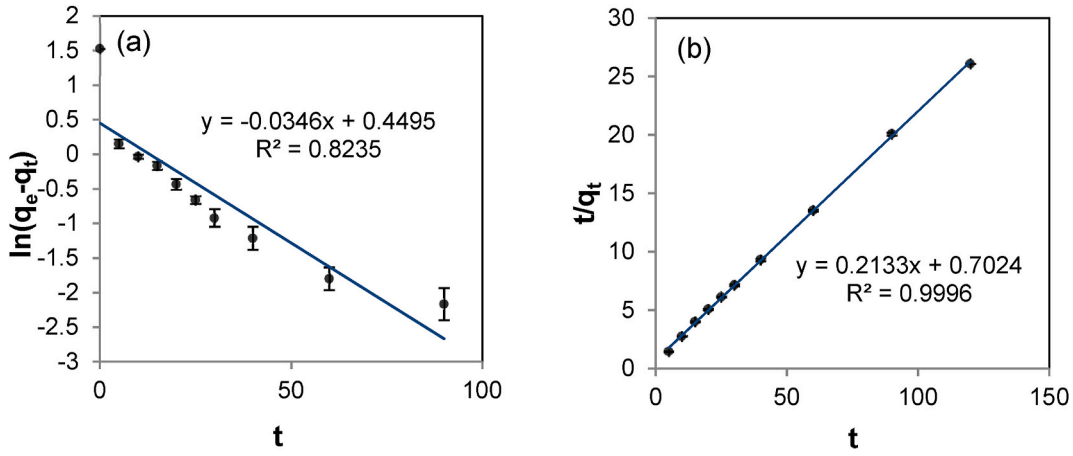

Fig. 9. Plot of kinetics models (a) PFO (b) PSO.

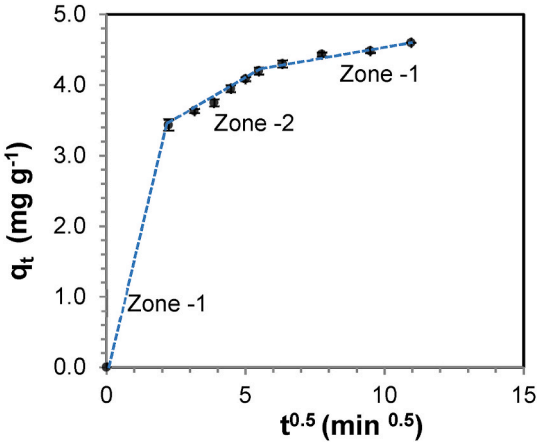

Fig. 10. Plot of IPD model.

identified as the dominant removal mechanisms. Further, this was confirmed by the reduction in the depth of O–H band in FTIR spectra of NaOH/Fe-MFA after fluoride adsorption (Fig. 7 (b)). Moreover, EDX results show a minor amount (0.54% by weight) of Mg^{2+} on NaOH/Fe-MFA surface, so involvement of Mg^{2+} is unlikely to occur. Also, iron oxide in the NaOH/Fe-MFA surface is deposited in amorphous form (from XRD), therefore surface Fe^{3+} ions are more reactive and easily adsorb fluoride ions. Thus, surface Fe^{3+} offers more active sites than Al^{3+}. This implied that fluoride adsorption by NaOH/Fe-MFA occurs mainly due to ion exchange with surface OH^- bond to Fe^{3+} active sites.

4. Conclusions

This study focuses on the development of novel adsorbent material by modifying RFA with NaOH followed by Fe^{3+} ions. Characterization results confirm the change in chemical composition, surface area, and pore distribution of adsorbents. Batch adsorption experiments revealed that NaOH/Fe-MFA has a greater adsorption capability than RFA. The maximum fluoride removal of 92% was achieved by NaOH/Fe-MFA at pH 2 under the optimum reaction conditions. At pH 7, 34% of removal was observed under the same conditions. Fluoride adsorption from NaOH/Fe-MFA was followed Langmuir isotherm, and monolayer adsorption on homogeneous surface was confirmed with a considerably high capacity of 18.6 mg g^{-1}. Also, chemisorption adsorption was revealed from well-fitted kinetics data with PSO kinetics model. Therefore, it can be concluded that under optimum conditions fluoride adsorption by NaOH/Fe-MFA occurs mainly due to ion exchange with surface OH^- bond to Fe^{3+} active sites. This study establishes the applicability of NaOH/Fe-MFA as a promising fluoride removal technique for industrial wastewater and also the effectiveness as a pre-treatment technique for contaminated groundwater.

Further, it is recommended to perform cyclic sorption-desorption studies, fixed-bed column breakthrough experiments, adsorption experiments using real water samples and also to conduct leaching studies during adsorption experiments.

Declaration of competing interest

The authors declare that they have no known competing financial interests or personal relationships that could have appeared to influence the work reported in this paper.

Acknowledgments

Authors are grateful to NORAD Waso - Asia project for providing resources and funds for the research work and to Prof. Rohan Weerasooriya of the National Institute of Fundamental Studies (NIFS), Sri Lanka, for the assistance given during the study.

Appendix A. Supplementary data

Supplementary data to this article can be found online at https://doi.org/10.1016/j.gsd.2021.100699.

References

Abaei, Z., Faghihian, H., Esmaeeli, N., 2017. Preparation and application of zeolitic adsorbents for removal of fuoride from aqueous solution; equilibrium, kinetic and thermodynamic studies. Chem. Sin. 8 (6), 524–534. https://www.imedpub.com/articles/preparation-and-application-of-zeolitic-adsorbents-for-removal-of-fuoride-fromaqueous-solution-equilibrium-kinetic-and-thermodynam.php?aid=21393.

Ahmed, S., et al., 2016. Geographical spread of fly ash generation and residual potential for its utilization in India. Int. J. Inf. Retr. Res. (IJIRR) 4 (1), 8–19. https://www.cibtech.org/J-Innovative-Research-Review/Publications/2016/VOL-4-NO-1/02-JIRR-002-SIRAJUDDIN-GEOGRAPHICAL.pdf.

Ali, S., et al., 2019. Concentration of Fluoride in Groundwater of India: A Systematic Review,meta-Analysis and Risk Assessment, vol. 9. Groundwater for Sustainable Development, p. 100224. https://doi.org/10.1016/j.gsd.2019.100224.

Ali, S., et al., 2018. Elevated fluoride in groundwater of Siwani Block, Western Haryana, India: a potential concern for sustainable water supplies for drinking and irrigation. Groundwater for Sustainable Development 7, 410–420. https://doi.org/10.1016/j.gsd.2018.05.008.

Aljeboree, A.M., Alshirifi, A.N., Alkaim, A.F., 2014. Kinetics and equilibrium study for theadsorption of textile dyes on coconut shell activated carbon. Arabian Journal of Chemistry 10, 3381–3393. https://doi.org/10.1016/j.arabjc.2014.01.020.

Apua, M.C., Simatea, G.S., 2018. Characterization of Coal Fly Ash for the Production of Coagulant for Usage in Wastewater Treatment. Materials Science and Technology Conference. https://doi.org/10.7449/2018/MST_2018_1512_1521. Columbus, Ohio, USA, October 14-18.

Byrappa, K., Kumar, B.V.S., 2007. Characterization of zeolites by infrared spectroscopy. Asian J. Chem. 6, 4933–4935. http://www.asianjournalofchemistry.co.in/User/ViewFreeArticle.aspx?ArticleID=19_6_118.

Chandrajith, R., et al., 2012. Spatial distribution of fluoride in groundwater of Sri Lanka. J. Natl. Sci. Found. Sri Lanka 40, 303–309. https://doi.org/10.4038/jnsfsr.v40i4.5044.

Clara, J.J., Kumar, S.P., 2016. Study of SEM/EDXS and FTIR for fly ash to determine the chemical changes of ash in marine environment. Int. J. Sci. Res. 5, 1688–1693. https://www.ijsr.net/search_index_results_paperid.php?id=ART2016554.

Coates, J., 2000. Interpretation of infrared spectra, A practical approach. In: Meyers, R.A. (Ed.), Encyclopedia of Analytical Chemistry. John Wiley & Sons Ltd., Chichester, pp. 10815–10837. https://doi.org/10.1002/9780470027318.a5606.

Dissanayake, C.B., 2005. Water quality in the dry zone of Sri Lanka - some interesting health aspects. J. Natl. Sci. Found. Sri Lanka 33 (3), 161–168. https://doi.org/10.4038/jnsfsr.v33i3.2322.

Elessawy, N.A., et al., 2020. One-pot green synthesis of magnetic fullerene nanocomposite for adsorption characteristics. Journal of Water Process Engineering 34, 101047. https://doi.org/10.1016/j.jwpe.2019.101047.

Fito, J., Said, H., Feleke, S., Worku, A., 2019. Fluoride removal from aqueous solution onto activated carbon of Catha edulis through the adsorption treatment technology. Environmental Systems Research 8, 25. https://doi.org/10.1186/s40068-019-0153-1.

Geethamani, C.K., et al., 2014. Alkali-treated fly ash for the removal of fluoride from aqueous solutions. Desalination and Water Treatment 52, 3466–3476. https://doi.org/10.1080/19443994.2013.800825.

Jacks, G., Bhattacharya, P., Chaudhary, V., Singh, K.P., 2005. Controls on the genesis of some high-fluoride groundwaters in India. Appl. Geochem. 20 (2), 221–228. https://doi.org/10.1016/j.apgeochem.2004.07.002.

Jayarathna, L., Bandara, A., Ng, W.J., Weerasooriya, R., 2015. Fluoride adsorption on γ − Fe2O3 nanoparticles. J. Environ. Health 13, 54. https://doi.org/10.1186/s40201-015-0210-2.

Kimambo, V., et al., 2019. Fluoride occurrence in groundwater systems at global scale and status of defluoridation – state of the art. Groundwater for Sustainable Development 9, 100223. https://doi.org/10.1016/j.gsd.2019.100223.

Kofa, G.P., et al., 2017. Removal of fluoride from water by adsorption onto fired clay pots: kinetics and equilibrium studies. J. Appl. Chem. 6254683. https://doi.org/10.1155/2017/6254683, 2017.

Koshy, N., Singh, D.N., 2016. Fly ash zeolites for water treatment applications. Journal of Environmental Chemical Engineering 4, 1460–1472. https://doi.org/10.1016/j.jece.2016.02.002.

Kumar, M., et al., 2016. Co-occurrence perspective of arsenic and fluoride in the groundwater of Diphu, Assam, Northeastern India. Chemosphere 150, 227–238. https://doi.org/10.1016/j.chemosphere.2016.02.019.

Kut, K.M.K., et al., 2016. A Review of Fluoride in African Groundwater and Local Remediation Methods, vols. 2–3. Groundwater for Sustainable Development, pp. 190–212. https://doi.org/10.1016/j.gsd.2016.09.001.

Largittea, L., Pasquier, R., 2016. A review of the kinetics adsorption models and their application to the adsorption of lead by an activated carbon. Chem. Eng. Res. Des. 109, 495–504. https://doi.org/10.1016/j.cherd.2016.02.006.

Maity, J.P., et al., 2018. Removal of fluoride from water through bacterial-surfactin mediated novel hydroxyapatite nanoparticle and its efficiency assessment: adsorption isotherm, adsorption kinetic and adsorption Thermodynamics. Environmental Nanotechnology, Monitoring & Management 9, 18–28. https://doi.org/10.1016/j.enmm.2017.11.001.

Makgabutlane, B., et al., 2020. Microwave-assisted synthesis of coal fly ash-based zeolites for removal of ammonium from urine. RSC Adv. 10, 2416–2427. https://doi.org/10.1039/C9RA10114D.

Mondal, N.K., Bhaumik, R., Datta, J.K., 2016. Fluoride adsorption by calcium carbonate, activated alumina and activated sugarcane ash. Environmental Processes 3, 195–216. https://doi.org/10.1007/s40710-016-0130-x.

Mozgawa, W., Król, M., Dyczek, J., Deja, J., 2014. Investigation of the coal fly ashes using IR spectroscopy. Spectrochim. Acta Mol. Biomol. Spectrosc. 132, 889–894. https://doi.org/10.1016/j.saa.2014.05.052.

Nie, G.H., et al., 2014. Effect of fluoride ion on floatation behavior of carbonate minerals and its mechanism. Zhonggu Youse Jinshu Xueboo/Chinese Journal of Nonferrous Metals 24, 3136–3141. http://cjonm.csu.edu.cn/paper/paperView.aspx?id=paper_308437.

Noor-ul-Amin, 2014. A multi-directional utilization of different ashes. RSC Adv. 4, 62769. https://doi.org/10.1039/C4RA06568A.

Panda, L., Kar, B., Dash, S., 2018. Preparation of fly ash based zeolite for removal of fluoride from drinking water. AIP Conference Proceedings 1953, 080003. https://doi.org/10.1063/1.5032809.

Pathiraja, G.C., et al., 2015. Investigating the surface characteristics of chemically modified and unmodified rice husk ash; bottom-up approach for adsorptive removal of water contaminants. Desalination and Water Treatment 54, 547–556. https://doi.org/10.1080/19443994.2014.883133.

Peiris, C., et al., 2019. The influence of three acid modifications on the physicochemical characteristics of tea-waste biochar pyrolyzed at different temperatures: a comparative study. RSC Adv. 9, 17612–17622. https://doi.org/10.1039/C9RA02729G.

Pengthamkeerati, P., Satapanajaru, T., Chularuengoaksorn, P., 2008. Chemical modification of coal fly ash for the removal of phosphate from aqueous solution. Fuel 87, 2469–2476. https://doi.org/10.1016/j.fuel.2008.03.013.

Prasad, B., Sangita, K., Tewary, B.K., 2011. Reducing the hardness of mine water using transformed fly ash. Mine Water Environ. 30, 61–66. https://doi.org/10.1007/s10230-010-0130-4.

Prasetyo, T.A.B., Soegijono, B., 2018. Characterization of sonicated natural zeolite/ferric chloride hexahydrate by infrared spectroscopy. J. Phys. Conf. 985, 012022 https://doi.org/10.1088/1742-6596/985/1/012022.

Qiu, M., et al., 2016. Effects of activation and modification on the microstructure and composition of fly ash. Am. Chem. Sci. J. 14, 1–6. https://doi.org/10.9734/ACSJ/2016/26348.

Rondón, W., et al., 2013. Application of 3A zeolite prepared from Venezuelan kaolin for removal of Pb (II) from wastewater and its determination by flame atomic absorption spectrometry. Am. J. Anal. Chem. 4, 584–593. https://doi.org/10.4236/ajac.2013.410069.

Sahoo, P.K., Tripathy, S., Panigrahi, M.K., Equeenuddin, S.M., 2013. Evaluation of the use of an alkali modified fly ash as a potential adsorbent for the removal of metals from acid mine drainage. Appl Water Science 3, 567–576. https://doi.org/10.1007/s13201-013-0113-2.

Salifu, A., 2017. Fluoride Removal from Groundwater by Adsorption Technology. Ph.D. Thesis, Delft University of Technology, Delft, the Netherlands. https://www.un-ihe.org/sites/default/files/2017_unesco-ihe_phd_thesis_salifu_i_0.pdf.

Suhartana Sukmasari, E., Azmiyawati, C., 2018. Modification of natural zeolite with Fe (III) and its application as adsorbent chloride and carbonate ions. IOP Conf. Ser. Mater. Sci. Eng. 349, 012075 https://doi.org/10.1088/1757-899X/349/1/012075.

Sun, Y., et al., 2011. Removal of fluoride from drinking water by natural stilbite zeolite modified with Fe(III). Desalination 277, 121–127. https://doi.org/10.1016/j.desal.2011.04.013.

Tan, K.L., Hameed, B.H., 2017. Insight into the adsorption kinetics models for the removal of contaminants from aqueous solutions. Journal of the Taiwan Institute of Chemical Engineers 74, 25–48. https://doi.org/10.1016/j.jtice.2017.01.024.

Tian, Z., Gan, Y., 2019. In situ synthesis of structural hierarchy flowerlike zeolite and its application for fluoride removal in aqueous solution. J. Nanomater. 2932973. https://doi.org/10.1155/2019/2932973, 2019.

Treacy, M.M.J., Higgins, J.B., 2001. Collection of Simulated XRD Powder Patterns for Zeolites Fourth Revised Edition. ELSEVIER. https://doi.org/10.1016/B978-0-444-53067-7.X5470-7.

Venuja, S., Mathiluxsan, S., Nasvi, M.C.M., 2017. Geotechnical engineering properties of peat, stabilized with a combination of fly ash and well graded sand. Engineer (12), 21–27. https://doi.org/10.4038/engineer.v50i2.7249.

Visa, M., Isac, L., Duta, A., 2012. Fly ash adsorbents for multi-cation wastewater treatment. Appl. Surf. Sci. 258, 6345–6352. https://doi.org/10.1016/j.apsusc.2012.03.035.

Vithanage, M., Bhattacharya, P., 2015. Fluoride in drinking water:health effects and remediation. In: Lichtfouse, E., Schwarzbauer, J., Robert, D. (Eds.), Environmental Chemistry for a Sustainable World: Volume 5: CO2 Sequestration, Biofuels and Depollution. Springer International Publishing, Switzerland, pp. 105–151.

Vithanage, M., Bhattacharya, P., 2015 b. Fluoride in the environment: sources, distribution and defluoridation. Environ. Chem. Lett. 13, 131–147. https://doi.org/10.1007/s10311-015-0496-4.

Waghmare, S., et al., 2015. Adsorption behaviour of modified zeolite as novel adsorbents for fluoride removal from drinking water: surface phenomena, kinetics and thermodynamics studies. International Journal of Science, Engineering and Technology Research 4, 4114–4124. http://ijsetr.org/wp-content/uploads/2015/12/IJSETR-VOL-4-ISSUE-12-4114-4124.pdf.

World Health Organization, 2004. Fluoride in Drinking Water, Background Document for Development of WHO Guidelines for Drinking-Water Quality. https://www.who.int/water_sanitation_health/dwq/chemicals/fluoride.pdf.

Worch, E., 2012. Adsorption Technology in Water Treatment. Dresden, Germany. https://doi.org/10.1515/9783110240238.

Xu, X., et al., 2011. Adsorption of fluoride from aqueous solution on magnesia-loaded fly ash cenospheres. Desalination 272, 233–239. https://doi.org/10.1016/j.desal.2011.01.028.

Yehia, A., Ezzat, K., 2009. Fluoride ion uptake by synthetic apatites. Adsorpt. Sci. Technol. 27 (3), 337–347. https://journals.sagepub.com/doi/pdf/10.1260/026361709789868910.

Zhang, M., et al., 2016. Coal fly ash/$CoFe_2O_4$ composites: a magnetic adsorbent for the removal of malachite green from aqueous solution. RSC Adv. 6, 93564–93574. https://doi.org/10.1039/C6RA08939A.